ACS APPLIED MATERIALS & INTERFACES

Research Article

www.acsami.org

Hierarchically Structured Suspended TiO_2 Nanofibers for Use in UV and pH Sensor Devices

Won Seok Lee, Yang-Seok Park, and Yoon-Kyoung Cho*

Department of Biomedical Engineering, School of Life Sciences, Ulsan National Institute of Science and Technology (UNIST), Banyeon-ri 100, Ulsan, 689-798, Republic of Korea

Supporting Information

ABSTRACT: Photoelectrochemical sensors based on hierarchically structured titanium dioxide (TiO_2) nanofibers (NFs) were fabricated by combination of electrospinning, carbon microelectromechanical systems (MEMS), and hydrothermal reaction. During the electrospinning step, a rotating drum collector was used to align and position NFs of titanium tetraisopropoxide (TTIP) in polyvinylpyrrolidone (PVP) on top of a carbon-MEMS structure. Following calcination under vacuum, a stable ohmic contact was obtained between suspended TiO_2-carbon NFs (TiO_2/C NF) and the carbon electrodes. Subsequent to this, a hierarchical nanostructure of TiO_2 nanowires (TiO_2 NWs) was hydrothermally synthesized onto the TiO_2/C NFs and successfully utilized as UV and pH sensors. This is the first demonstration of a semiconductor-based nanofiber sensor suspended on carbon electrodes that has been achieved by a relatively simple and cost-effective electrospinning method. Furthermore, these sensors demonstrate a high sensitivity, as well as a stable ohmic contact, due to the large surface area of the TiO_2 NWs and the carbon−carbon contact between the suspended TiO_2/C NFs and carbon electrodes.

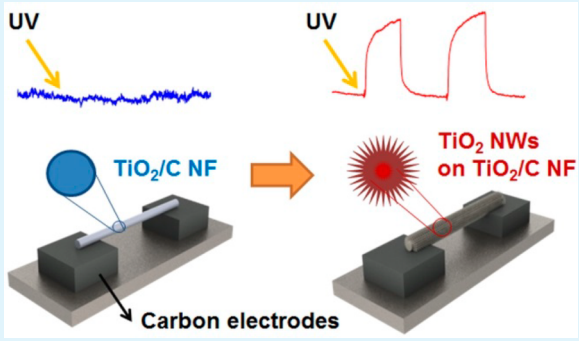

KEYWORDS: *semiconductor nanofiber, direct alignment, electronic device, UV and pH sensor*

INTRODUCTION

Semiconducting nanoelectronic devices have attracted considerable attention in recent years due to their unique photoelectrochemical properties.[1,2] In particular, titanium dioxide (TiO_2) has proven to be the material of choice for various applications such as sensors,[3−5] transistors,[6] solar cells,[7,8] water splitting,[9] and antimicrobial agents[10] by virtue of its electron band structure, high sensitivity, low cost, rapid response time, and recovery behavior; as well as providing photo/chemical stability and biocompatibility.

Field effect transistor (FET)-type nanoelectronic devices can be achieved through the integration of TiO_2 nanomaterials produced by chemical vapor deposition (CVD),[11,12] sol−gel,[13] chemical precipitation,[14] and hydrothermal synthesis.[15,16] Furthermore, as an alternative to patterning such nanomaterials on a substrate, three-dimensional nanostructures such as suspended nanowires can provide enhanced sensitivity through their much greater surface area. As such, various efforts have already been made to fabricate suspended structures;[17−23] however, these methods have thus far required complex integration processes, such as the precise transfer and alignment of nanomaterials onto prepatterned metal electrodes using dielectrophoresis (DEP),[17−19,23] magnetic fields,[20] manipulation by electrostatic force,[21,24] or contact printing.[25] Although these methods can integrate and suspend nanomaterials onto prepatterned metal electrodes, the contact between the nanomaterials and metal electrodes achieved is unstable due to a weak force of adhesion. This, in turn, causes electrical instability and mechanical failures that are driven by thermal or mechanical stress. The end result is that postbonding processes such as selective metal deposition by focused ion beam (FIB),[21,26] soldering,[20] metal deposition by photolithography,[19] and compression[22,23,27] are invariably required to ensure a mechanically and electrically stable contact for reliable operation. However, this requirement for serial processes greatly increases the cost, time, and complexity of manufacturing, thereby reducing throughput to levels that make it difficult to economically achieve reliable devices on a commercial scale.

In contrast, nanomaterials can be directly deposited onto electrodes via electrostatic spray deposition (ESD)[28,29] or electrospinning (ES) technique.[30,31] In particular, ES presents a simple, fast, and low-cost technique for fabricating nanofibers (NFs) of various materials (including polymers, carbon, and semiconductors) and can therefore provide a straightforward way to assemble and integrate NFs onto electrodes without the need for a complex transfer and alignment process.[32] Typically, electrospun NFs are deposited onto a grounded substrate in a random orientation; however, a high degree of alignment can be achieved by using a rotating drum collector, in which NFs are oriented in the direction of rotation by being stretched as

Received: March 14, 2014
Accepted: July 10, 2014
Published: July 10, 2014

   dx.doi.org/10.1021/am501563v | ACS Appl. Mater. Interfaces 2014, 6, 12189−12195

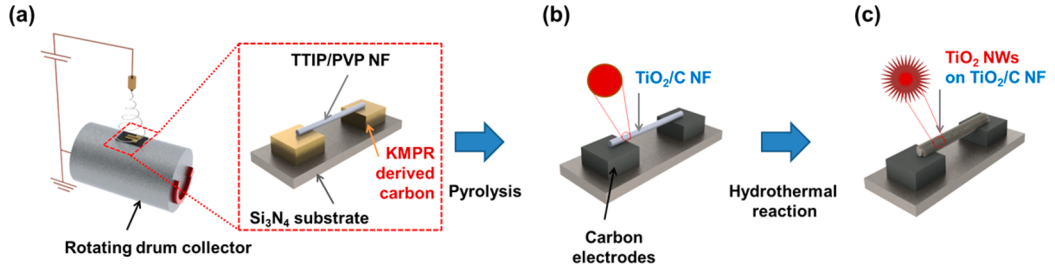

Figure 1. Fabrication of hierarchically structured TiO_2 NWs on TiO_2/C NFs suspended and aligned on carbon electrodes: (a) Electrospun TTIP/PVP NFs are suspended on carbon electrodes prepared by the pyrolysis of a photopatterned KMPR resist at 500 °C. (b) A stable ohmic contact between the TiO_2/C NFs and carbon electrodes is obtained following pyrolysis at 900 °C. (c) TiO_2 NWs are hydrothermally synthesized on the suspended TiO_2/C NFs.

they are deposited on the substrate.[33] Recently, Sharma et al. reported that polymer NFs suspended on a SU-8 photopatterned microelectromechanical systems (MEMS) structure can be achieved by using a rotating drum collector.[34] Moreover, both the polymer NFs and the MEMS structure of the SU-8 photoresist were carbonized by pyrolysis, thus resulting in a stable ohmic contact. This behavior is advantageous, in that it means nanoelectronic devices can be readily achieved through a simple ES and pyrolysis process, without the necessity for complicated and expensive alignment and postbonding steps. Its application to carbon-based electronic devices is, however, inherently limited by the zero band gap of the material.

In this study, this methodology is expanded to the development of semiconductor-based suspended NFs. To this end, suspended TiO_2−carbon NFs (TiO_2/C NFs) are prepared, and the ohmic contact between these NFs and the carbon electrodes is investigated. In addition, hydrothermal synthesis was employed to obtain a hierarchical structure of TiO_2 NWs on the previously suspended TiO_2/C NFs. The aim of this was to increase the detection sensitivity by increasing the surface area, thus potentially enabling their use in ultraviolet (UV) and pH sensors.

EXPERIMENTAL SECTION

Materials. Titanium tetraisopropoxide (TTIP, 98%), polyvinylpyrrolidone (PVP, M_w = 1 300 000), acetic acid, anhydrous ethanol (99.5+%), and titanium butoxide ($Ti(OBu)_4$, 97%) were all purchased from Sigma-Aldrich. KMPR 1035 was purchased from MicroChem, and hydrochloric acid (HCl, 35−37%) was purchased from Samchun.

Fabrication of Carbon MEMS Structure. Photopatterned KMPR resist fabricated by conventional photolithography was pyrolyzed to prepare carbon-MEMS structures. The process is briefly described as follows. First, a KMPR resist was spin-coated onto a Si_3N_4 dielectric layer (300 nm) that had been previously deposited on a Si substrate using low pressure chemical vapor deposition (LPCVD) at 2800 rpm. Following soft-baking at 100 °C for 20 min, photolithography under UV light with a peak wavelength of λ = 365 nm at 850 mJ/cm^2, postbaking at 100 °C for 4 min, and development processes for 15 min, a MEMS structure with a gap distance of 10 μm and height of 55.39 ± 1.27 μm was obtained, as shown in Supporting Information Figure S1 and Table S1. After pyrolysis for 3 h at 500 °C, with a heating rate of 1 °C/min under vacuum conditions of ∼5 × 10^{-7} Torr, a KMPR-derived carbon-MEMS structure with a gap distance of 75.33 ± 1.89 μm and height of 10.26 ± 0.54 μm was obtained.

Fabrication of Suspended TiO_2/C NFs on Carbon Electrodes. TiO_2/C NFs were obtained by the ES of TTIP/PVP NFs and their subsequent pyrolysis. The detailed procedure is as follows. First, a precursor solution was prepared by mixing TTIP (1.5 g) dissolved in ethanol (3 mL) and acetic acid (3 mL) with a solution containing 11 wt % PVP in ethanol. The solution was loaded in a syringe with stainless steel needle with a diameter of 400 μm, which was connected to a syringe pump set with the flow rate of 0.5 mL/h. The KMPR-derived carbon MEMS structure was affixed on a grounded drum, which rotates during the ES with the spin speed of 2500 rpm. For the ES process, a high DC voltage (15 kV) was applied between the needle and the drum, the distance of which was fixed at 10 cm. Figure 1a shows a schematic diagram depicting TTIP/PVP NFs suspended and aligned in a uniaxial direction on the carbon-MEMS structure derived from KMPR. To place the TTPIP/PVP NFs on the desired location of the carbon-MEMS structure, the other region was masked by polyimide film. After the ES process, the polymer film was detached, and TTIP/PVP NFs deposited at the desirable location on the carbon-MEMS structure could be obtained. Following a second pyrolysis at 900 °C for 3 h, with a heating rate of 1 °C/min under vacuum conditions of ∼5 × 10^{-7} Torr, TiO_2/C NFs were obtained on the carbon electrodes, as illustrated in Figure 1b. These TiO_2/C NFs had a diameter of 100−150 nm (Supporting Information Figure S2), while the carbon electrodes had a gap distance of 77.00 ± 0.82 μm and height of 7.84 ± 0.36 μm (Supporting Information Figure S1 and Table S1).

Synthesis of Hierarchically Structured TiO_2 NWs. The hierarchical structure of the TiO_2/C NFs was achieved by synthesizing TiO_2NWs onto the TiO_2/C NFs suspended and aligned on carbon electrodes, as shown in Figure 1c. This synthesis was performed as follows: 1.7 mL of $Ti(OBu)_4$ was injected into a 5.83 M HCl solution, and then stirred for 10 min. Following this, a device consisting of TiO_2/C NFs aligned and suspended on carbon electrodes was immersed into the mixture at an angle, so as to ensure that the TiO_2/C NFs were facing downward. This was then sealed in an autoclave and kept at 150 °C for 6 h. After the temperature was naturally cooled to room temperature (23 °C), the device was washed with DI water and ethanol.

Characterization. Field-emission scanning electron microscopy (FE-SEM, FEINano230) was used for the microstructural characterization of the suspended TiO_2/C NF and TiO_2 NWs-TiO_2/C NF-based device, respectively. A probe station (MST-8000C, MSTech) was used for the electrical characterization, in which two sharp probe tips were contacted onto two carbon electrodes, respectively. I−V characteristics of the device then were measured by direct-current voltage sweeping mode by using a semiconductor analyzer (4200-SCS, Keithley). X-ray photoelectron spectroscopy (XPS, K-alpha) and X-ray diffraction (XRD, D8 Advance, Bruker) were used to confirm the elemental composition and crystal phases of the TiO_2/C NFs and TiO_2 NWs.

UV and pH Sensing Experiment. For the UV sensing experiment, a UV lamp with a light intensity of 0.7 mW/cm^2 and peak wavelength of λ = 365 nm was used. The UV lamp was placed with a distance of 20 cm on TiO_2 NWs-TiO_2/C NF-based device and switched on and off repeatedly with the time periods of 35 s. Changes in electrical current measured through the TiO_2 NWs-TiO_2/C NF that occurred upon the exposure to UV were measured using a probe station at a constant DC bias of 1 V. For the pH sensing experiment, phosphate buffer solutions were made to different pH values by mixing 10 mM phosphate buffer (pH 7.4) to an appropriate ratio with either

0.1 M HCl or 0.1 M NaOH, and the pH of the resulting solution was confirmed by a pH meter (Fisher Accumet AR10). The region of TiO_2 NWs-TiO_2/C NF was dipped into the prepared solution with varying pH values, and changes in electrical current through the TiO_2 NWs-TiO_2/C NF were measured using a probe station at a constant DC bias of 1 V.

RESULTS AND DISCUSSION

The rotational speed of the drum collector was controlled between 500 and 2500 rpm, so as to highly align and position TTIP/PVP NFs onto a Si substrate. At 500 rpm, the TTIP/PVP NFs were deposited without a fixed oriented direction, as shown in Figure 2a. On the other hand, as the rotation speed of the drum collector was increased to 2500 rpm, the TTIP/PVP NFs became more oriented in the direction of rotation, as shown in Figure 2b. This alignment was attributed to the fact that when TTIP/PVP NFs are deposited onto a drum collector rotated at sufficient speed, they undergo a mechanical pulling that results in a high degree of alignment.[33]

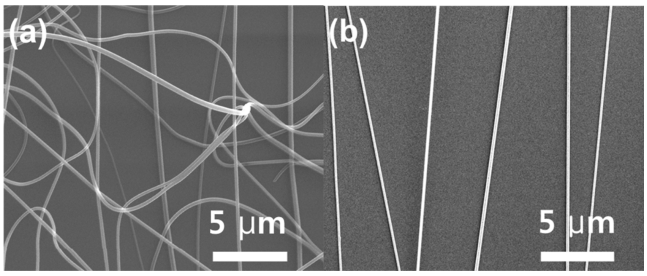

Figure 2. Comparison of drum collector rotation speeds at 15 kV, a flow rate of 0.5 mL/h, and a fixed distance of 10 cm between the drum collector and needle: (a) TTIP/PVP NFs are deposited onto a Si substrate with a random orientation at a drum speed of 500 rpm. (b) TTIP/PVP NFs are deposited in a uniaxial direction at a drum speed of 2500 rpm.

Knowing the conditions required for alignment made it possible to then directly assemble uniaxially orientated TTIP/PVP NFs onto the KMPR-derived carbon MEMS structure. For this, the KMPR resist patterned on a Si_3N_4/Si substrate was affixed to a drum collector rotated at 2500 rpm during the ES of TTIP/PVP NFs. This was then carbonized by pyrolysis to yield TiO_2/C NFs and carbon electrodes; however, some breakage of the TiO_2/C NFs suspended on the carbon electrodes was found to occur as a result of this process. As shown in Figure 3a,b, this breakage was caused by shrinkage of the KMPR resist during pyrolysis due to its carbonization,[34] thus resulting in an increase in the gap distance between the carbon electrodes from 10 μm to 77 $\pm$ 0.82 μm (Supporting Information Figure S1 and Table S1). The mechanical stretching that this induces provides the force needed to break the TiO_2/C NFs, as shown in Figure 3b. To prevent this breakage of the TiO_2/C NFs, the pyrolysis process was modified to incorporate into two steps, as follows: First, the KMPR-derived carbon MEMS structure was only partially pyrolyzed at 500 °C for 3 h, prior to the assembly of TTIP/PVP NFs on its surface. As shown in Figure 3c, this results in an increase in the gap distance to 75.33 $\pm$ 1.89 μm (Supporting Information Figure S1 and Table S1). Second, following the assembly of TTIP/PVP NFs on the KMPR-derived carbon MEMS structure surface, it is pyrolyzed at 900 °C for 3 h. This successfully prevented breakage of the TiO_2/C NFs, as shown in Figure 3d, while still ensuring their suspension and alignment on the carbon electrodes by virtue of the greatly reduced gap increase of just 2 μm (Supporting Information Figure S1 and Table S1). We next measured the conductivity of the TiO_2/C NFs-based device. Because the number of TiO_2/C NFs was varied in the fabrication of device each time, we prepared single TiO_2/C NF suspended and aligned on the carbon electrodes by cutting extra TiO_2/C NFs by using a focused ion beam (FIB) milling system to avoid the broad distribution of conductivity value caused by the different number of TiO_2/C NF. This revealed a stable ohmic contact with a relatively low resistance of $7.54 \times 10^5 \pm 1.1 \times 10^5$ Ω, as shown in Figure 3e. We observed that the micropatterns pyrolyzed at 500 °C for 3 h were not conductive, which indicated that it was not fully carbonized. It became conductive

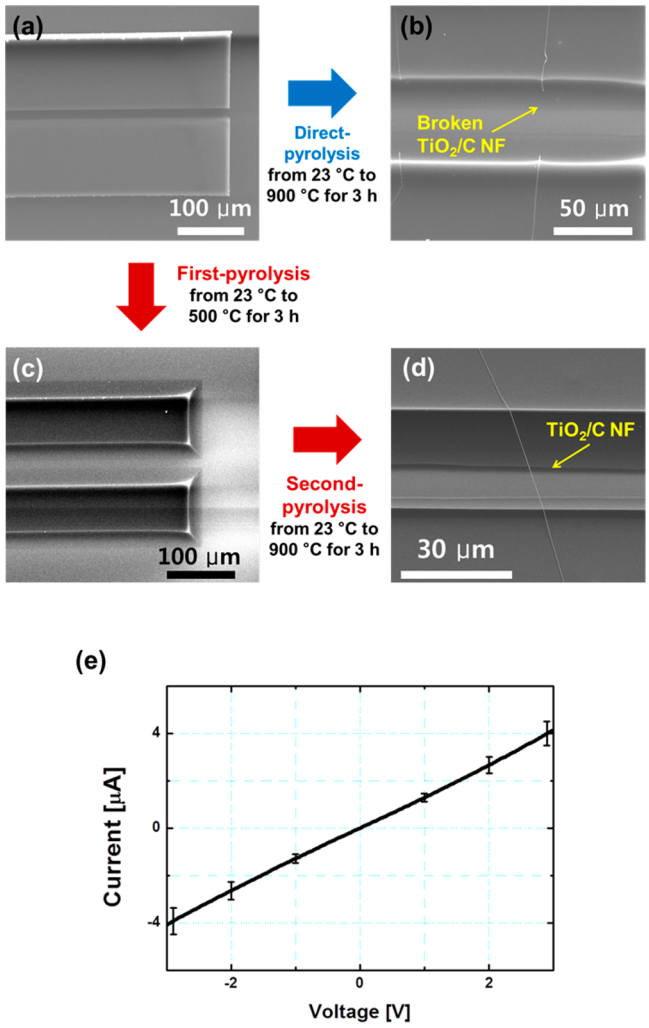

Figure 3. Comparison of pyrolysis processes for the carbonization of TTIP/PVP NFs and KMPR resist: (a) as-patterned KMPR resist with the two electrodes 10 μm apart; (b) direct-pyrolysis of the KMPR resist and TTIP/PVP NFs at 900 °C for 3 h causes breakage of the suspended TiO_2/C NFs due to an increase in the electrode gap to 77 $\pm$ 0.82 μm; (c) first-stage-pyrolysis of KMPR resist at 500 °C for 3 h before TTIP/PVP NFs are assembled on it, in which the gap distance is increased to 75.33 $\pm$ 1.89 μm; and (d) second-stage-pyrolysis of the partially pyrolyzed KMPR resist at 900 °C for 3 h after assembly of TTIP/PVP NFs. TiO_2/C NF breakage is eliminated due to the much smaller gap distance increase of just 2 μm (from 75.33 $\pm$ 1.89 to 77 $\pm$ 0.82 μm). (e) I_D–V_{DS} curve for a single TiO_2/C NF-based device, which reveals ohmic contact with a relatively low resistance value of $7.54 \times 10^5 \pm 1.1 \times 10^5$ Ω.

as the pyrolysis temperature was increased to 900 °C possibly due to the extensive graphitization process. In the current work, the ohmic contact could be formed when TTIP/PVP NFs were first deposited on the partially pyrolyzed micropattern and then fully carbonized together at 900 °C, which resulted in carbon-to-carbon contact between the fiber and the base MEMS structure. This suggests that the TiO_2/C NFs and carbon electrodes are well bonded by the carbon-to-carbon contact, in which the carbon component of the TiO_2 NFs is derived from PVP. The resistivity of a single TiO_2/C NF with a length of 77 μm and diameter of 130 nm was also calculated, returning a resistivity of $\rho = 1.45 \times 10^{-2}$ Ω cm that is significantly lower than the $\rho = 10^2$–10^7 Ω cm[35] of a polycrystalline TiO_2 film.

This low resistivity value for the TiO_2/C NFs was attributed to the predominance of carbon, as it was comparable to the $\rho = 5.42 \times 10^{-2}$ Ω cm of a single carbon NF.[34] The XPS analysis results shown in Supporting Information Figure S3 and Table S2 confirm that the TiO_2/C NFs consist mainly of carbon (53.27%), with a small amount of Ti (7.33%). However, although this carbonized TiO_2/C NF offers advantages such as a low resistivity, it is hindered by a poor photocatalytic performance relative to other TiO_2 materials. This is because the increase in carbon creates more defects and disordered phases in the crystalline structure of TiO_2, thus resulting in an amorphous TiO_2 phase in the carbonized NF.[36] In an effort to improve the crystallinity of the TiO_2, as well as increase the surface area of the NF, additional TiO_2 NWs were hydrothermally synthesized[5] onto the TiO_2/C NFs, with the originally deposited TiO_2 NFs acting as a seed material for TiO_2 NWs growth. A noteworthy result of this was that carbon electrodes derived from a SU-8 photoresist were found to be detached from a SiO_2 dielectric substrate, as shown in the Supporting Information Figure S4a. This was attributed to their weak adhesion,[37] especially under the acidic conditions required for hydrothermal synthesis using HCl. In using a KMPR resist on a Si_3N_4 dielectric substrate, this problem was successfully overcome by ensuring a much stronger force of adhesion, as shown in Supporting Information Figure S4b. The end result was that TiO_2 NWs with a diameter of ∼50 nm and length of ∼150 nm were successfully synthesized on the suspended and aligned TiO_2/C NFs on the carbon electrodes, as shown in Figure 4a. Characterization of the crystalline phases of this synthesized TiO_2 by XRD analysis is shown in Figure 4b, in which crystalline structures of TiO_2 are notably absent in the TiO_2/C NFs. This further indicates that the TiO_2 species existed as an amorphous phase due to the predominance of carbon. In contrast, crystal structures are clearly discernible in the TiO_2 NWs-TiO_2/C NFs due to single-crystal rutile TiO_2 NWs synthesized on the TiO_2/C NFs where the peaks at 27.48°, 36.18°, 41.28°, and 54.18° are well indexed as rutile crystal planes of (110), (101), (111), and (211). As shown in Figure 4c, the resistivity of a single TiO_2 NWs-TiO_2/C NF was calculated from the resistances obtained at different gap distances of 66.33 ± 3.09 and 77 ± 0.82 μm, these being derived from KMPR resists with initial gap distances of 5 and 10 μm, respectively (Supporting Information Figure S1 and Table S1). This revealed an increased resistivity of $\rho = 1.56$ Ω cm when compared to a single TiO_2/C NF, which is attributed to the increased loading of Ti from 7.33% to 16.29%, as shown in Supporting Information Figure S3 and Table S2. However, this value of $\rho = 1.56$ Ω cm is still significantly lower than the 10^2–10^7 Ω cm of a polycrystalline TiO_2 film, and comparable

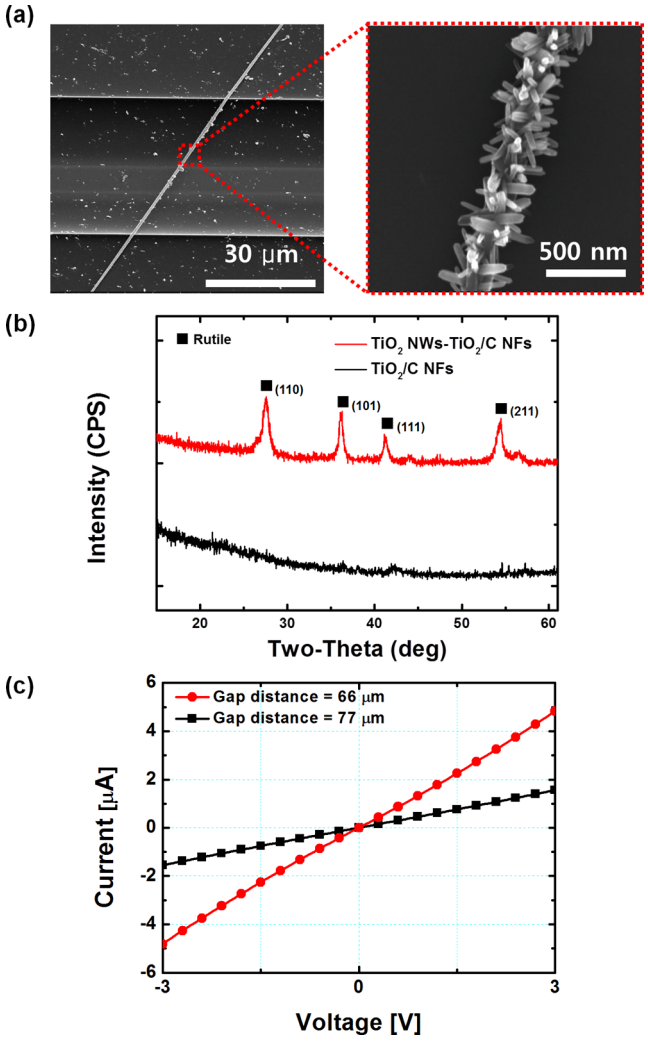

Figure 4. Microstructural and electrical characterization of TiO_2 NWs-TiO_2/C NF-based device: (a) SEM image of hierarchically structured TiO_2 NWs hydrothermally synthesized on TiO_2/C NF suspended on carbon electrodes. (b) XRD analysis of the TiO_2 NWs synthesized on the TiO_2/C NFs. The peaks are indexed as rutile in TiO_2 NWs-TiO_2/C NFs. (c) I_D–V_{DS} curve of a single TiO_2 NWs-TiO_2/C NF-based device for two different gap distances (66 and 77 μm). The resistivity of $\rho = 1.56$ Ω cm was calculated from these measurements.

to the $\rho = 1.09$ Ω cm of a single-crystal anatase TiO_2 nanotube.[38]

The applicability of the device as a UV and pH sensor is demonstrated at low DC bias of 1 V in Figure 5. From the UV sensing data shown in Figure 5a, it is clear that the TiO_2/C NF-based device is not photosensitive, a result of its noncrystalline structure and high number of defects such as oxygen vacancies. N.-L. Wu et al.[39] have also previously reported that the photocatalytic performance of TiO_2 powders becomes poor when they are calcinated under vacuum, which is due to a high number of oxygen vacancies inhibiting the transference of generated electrons and holes to the reactant surface under UV illumination. This, in turn, inevitably results in a recombination of the electron and hole pair. In contrast, the improved crystalline structure and TiO_2 loading of the TiO_2 NWs-TiO_2/C NF-based devices make them quite sensitive to UV light, with an average on/off ratio of 1.10 even at a low UV power density of 0.7 mW/cm^2 and a low DC bias of 1 V. This also represents a significant improvement over devices based on

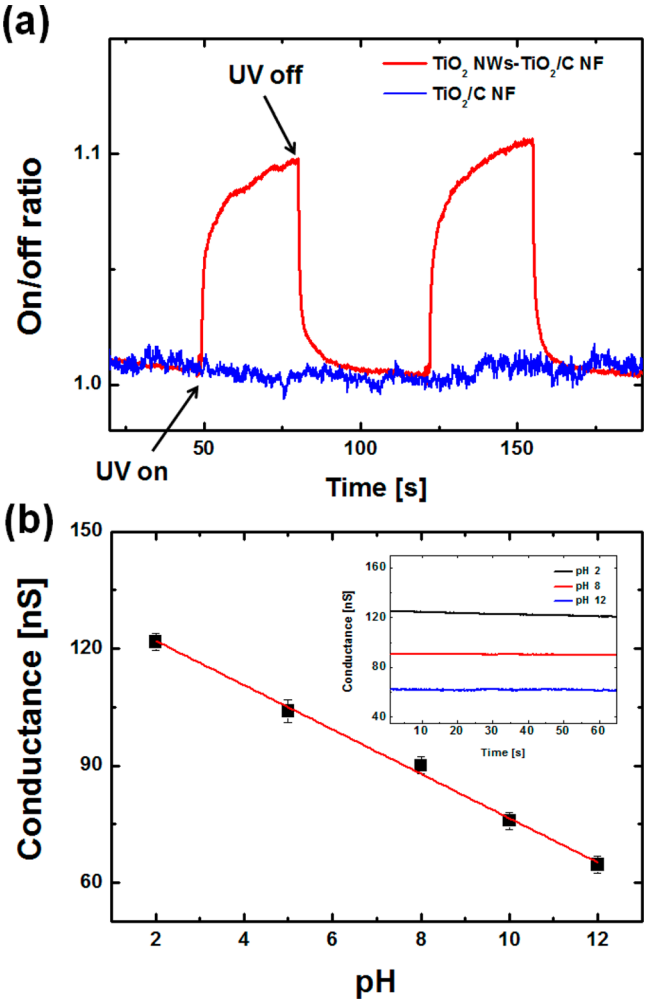

Figure 5. Application of hierarchically structured TiO_2 NWs-TiO_2/C NF suspended on a carbon-electrode-based electronic device as a UV and pH sensor: (a) response to UV light (λ = 365 nm) in ambient air at room-temperature, with a DC bias of 1 V; and (b) electrical conductance of TiO_2 NWs-TiO_2/C NF at a DC bias of 1 V and pH values of 2, 5, 8, 10, and 12. The red line is the linear fit through the data. (inset) Plot of conductance versus time at pH values of 2, 8, and 12.

electrospun ZnO NFs,[40] which are not sensitive to UV light even at a DC bias of 5 V. Under UV illumination, the conductance of the device was increased from 68 to 75 nA; however, this was reduced once the device was placed under conditions of darkness, with a recovery time of less than 0.1s. This phenomenon of increased electrical current is known to be due to the generation of free electrons in TiO_2 NWs under UV illumination, which thus leads to a decrease in resistivity.[4]

With regards to pH sensing, as shown in Figure 5b, the conductance of the device was measured under static conditions in buffer solutions of varying pH values. This found that the conductance linearly decreases with a resolution of 5.68 ± 0.28 nS/pH, at a constant DC bias of 1 V, as the pH level of the buffer solutions is increased from 2 to 12. This result is comparable to that obtained with a single Si NW, which exhibits a resolution of 5 nS/pH,[41] and can be attributed to the surface electron charge of n-type TiO_2 NWs by the surrounding ion charge concentration.[42] Specifically, at a low pH level of 2, the high concentration of H^+ ions in the solution reduces the depletion layer on the surface of the TiO_2 NWs, thus giving rise to an increase in the conductance of the device. In contrast, at a high pH level of 12, the high concentration of OH^- ions increases the depletion layer at the surface of the TiO_2 NWs, which leads to a reduced conductance.

These results successfully demonstrate the practical application of this device as a UV and pH sensor, and thus we believe that such devices fabricated by ES with a rotating drum collector and posthydrothermal synthesis can be widely applied to various nanoelectronic devices.

In this work, we employed a drum collector to provide a simple and efficient method to prepare relatively well-aligned NFs on one pair of electrodes. However, the precision of the positioning of the NFs can be further improved by applying an additional electric field either on the substrate[43,44] or between the tip and the substrates.[45]

CONCLUSIONS

This study has demonstrated that hierarchical TiO_2 NWs-TiO_2/C NFs suspended on carbon electrodes in a uniaxial direction can be achieved by combining electrospinning (ES) with a rotating drum collector, followed by controlled pyrolysis and hydrothermal synthesis. Although pyrolysis at 900 °C was found to cause breakage of the TiO_2/C NFs, this could be overcome by dividing the pyrolysis process into two steps: the first-stage-pyrolysis of KMPR resist at 500 °C prior to the assembly of TTIP/PVP NFs on its surface, and second-stage-pyrolysis at 900 °C after the assembly of TTIP/PVP NFs on the KMPR-derived carbon MEMS structure surface. The devices fabricated in this way exhibited good ohmic contact, with a low resistivity of $\rho = 1.45 \times 10^{-2}$ Ω cm. Subsequent hydrothermal synthesis of TiO_2 NWs on the TiO_2/C NFs formed a hierarchical structure, while also improving the crystalline structure of the TiO_2 and the surface area of the NFs. This resulted in a device that maintained a low resistivity of ρ = 1.56 Ω cm, and that could be successfully applied as a UV and pH sensor at DC bias of 1 V, demonstrating an average on/off ratio of 1.10 and a resolution of 5.68 ± 0.28 nS/pH as a UV and pH sensor, respectively. We believe that given the relatively low-cost and simplicity of this technology; made possible by the lack of complex transfer, alignment, and bonding processes, it has great potential for the fabrication of one-dimensional semiconductor-based electronic devices offering enhanced sensitivity for a variety of applications.

ASSOCIATED CONTENT

Supporting Information

(1) Microscopic analysis for the shrinkage of KMPR-resist after pyrolysis and (2) TiO_2/C NF suspended and aligned on carbon electrodes with the information on its diameter; (3) XPS analysis of the surface atomic composition of TiO_2/C NFs and TiO_2 NWs-TiO_2/C NFs; (4) images of carbon electrodes detached from SiO_2/Si substrate and remaining on Si_3N_4 substrate after hydrothermal synthesis of TiO_2 NWs; and (5) electrical characterization of the device without TiO_2 NFs. This material is available free of charge via the Internet at http://pubs.acs.org.

AUTHOR INFORMATION

Corresponding Author

*Tel.: +82-52-217-2511. Fax: +82-52-217-2509. E-mail: ykcho@unist.ac.kr.

Notes

The authors declare no competing financial interest.

■ ACKNOWLEDGMENTS

This work was supported by the National Research Foundation (NRF) grants (2010-0028684 and 2013R1A2A2A05004314) and by the Korean Health Technology R&D Project, Ministry of Health & Welfare (A121994), funded by the Korean government. We thank Prof. Marc Madou for helpful discussion on the fabrication of electrospun carbon nanofiber.

■ REFERENCES

(1) Alivisatos, A. P. Semiconductor Clusters, Nanocrystals, and Quantum Dots. *Science* **1996**, *271*, 933−937.
(2) Lu, W.; Xie, P.; Lieber, C. M. Nanowire Transistor Performance Limits and Applications. *IEEE Trans. Electron Devices* **2008**, *55*, 2859−2876.
(3) Zhu, Y.; Shi, J.; Zhang, Z.; Zhang, C.; Zhang, X. Development of a Gas Sensor Utilizing Chemiluminescence on Nanosized Titanium Dioxide. *Anal. Chem.* **2001**, *74*, 120−124.
(4) Cao, C.; Hu, C.; Wang, X.; Wang, S.; Tian, Y.; Zhang, H. UV Sensor Based on TiO2 Nanorod Arrays on FTO Thin Film. *Sens. Actuators, B* **2011**, *156*, 114−119.
(5) Sun, C.; Wang, N.; Zhou, S.; Hu, X.; Zhou, S.; Chen, P. Preparation of Self-Supporting Hierarchical Nanostructured Anatase/Rutile Composite TiO2 Film. *Chem. Commun.* **2008**, 3293−3295.
(6) Ishii, M.; Terauchi, M.; Yoshimura, T.; Nakayama, T.; Fujimura, N. Characterization of Field Effect Transistor with TiO2 Nanotube Channel Fabricated by Dielectrophoresis. *IOP Conf. Ser.: Mater. Sci. Eng.* **2011**, *18*, 082019.
(7) Stefik, M.; Heiligtag, F. J.; Niederberger, M.; Grätzel, M. Improved Nonaqueous Synthesis of TiO2 for Dye-Sensitized Solar Cells. *ACS Nano* **2013**, *7*, 8981−8989.
(8) Yun, H.-G.; Park, J. H.; Bae, B.-S.; Kang, M. G. Dye-Sensitized Solar Cells with TiO2 Nano-Particles on TiO2 Nano-Tube-Grown Ti Substrates. *J. Mater. Chem.* **2011**, *21*, 3558−3561.
(9) Wang, G.; Wang, H.; Ling, Y.; Tang, Y.; Yang, X.; Fitzmorris, R. C.; Wang, C.; Zhang, J. Z.; Li, Y. Hydrogen-Treated TiO2 Nanowire Arrays for Photoelectrochemical Water Splitting. *Nano Lett.* **2011**, *11*, 3026−3033.
(10) Chen, F.; Yang, X.; Xu, F.; Wu, Q.; Zhang, Y. Correlation of Photocatalytic Bactericidal Effect and Organic Matter Degradation of TiO2 Part I: Observation of Phenomena. *Environ. Sci. Technol.* **2009**, *43*, 1180−1184.
(11) Pradhan, S. K.; Reucroft, P. J.; Yang, F.; Dozier, A. Growth of TiO2 Nanorods by Metalorganic Chemical Vapor Deposition. *J. Cryst. Growth* **2003**, *256*, 83−88.
(12) Li, W.; Ismat Shah, S.; Huang, C. P.; Jung, O.; Ni, C. Metallorganic Chemical Vapor Deposition and Characterization of TiO2 Nanoparticles. *Mater. Sci. Eng., B* **2002**, *96*, 247−253.
(13) Su, C.; Hong, B. Y.; Tseng, C. M. Sol−Gel Preparation and Photocatalysis of Titanium Dioxide. *Catal. Today* **2004**, *96*, 119−126.
(14) Scolan, E.; Sanchez, C. Synthesis and Characterization of Surface-Protected Nanocrystalline Titania Particles. *Chem. Mater.* **1998**, *10*, 3217−3223.
(15) Zhang, Y. X.; Li, G. H.; Jin, Y. X.; Zhang, Y.; Zhang, J.; Zhang, L. D. Hydrothermal Synthesis and Photoluminescence of TiO2 Nanowires. *Chem. Phys. Lett.* **2002**, *365*, 300−304.
(16) Li, J.; Wan, W.; Zhou, H.; Li, J.; Xu, D. Hydrothermal Synthesis of TiO2(B) Nanowires with Ultrahigh Surface Area and their Fast Charging and Discharging Properties in Li-Ion Batteries. *Chem. Commun.* **2011**, *47*, 3439−3441.
(17) Robert, J. H.; Joseph, D. B.; Mark, A. E.; Bo, L.; Matthew, S. M.; Lu, S.; Jason, S.; Jeremy, A. S. Electrically Directed Assembly and Detection of Nanowire Bridges in Aqueous Media. *Nanotechnology* **2006**, *17*, S280−S286.
(18) Lu, S.; Tami Lasseter, C.; Mark, A. E.; Matthew, S. M.; Kevin, M. M.; Robert, J. H. Electrical Characterization of Nanowire Bridges Incorporating Biomolecular Recognition Elements. *Nanotechnology* **2005**, *16*, 2846−2851.
(19) Suh, D.-I.; Lee, S.-Y.; Hyung, J.-H.; Kim, T.-H.; Lee, S.-K. Multiple ZnO Nanowires Field-Effect Transistors. *J. Phys. Chem. C* **2008**, *112*, 1276−1281.
(20) Hongke, Y.; Zhiyong, G.; Yu, T.; Gracias, D. H. Integrating Nanowires with Substrates Using Directed Assembly and Nanoscale Soldering. *IEEE Trans. Nanotechnol.* **2006**, *5*, 62−66.
(21) Seung-Yong, L.; Gil-Sung, K.; Mi-Ri, L.; Hyuneui, L.; Wan-Doo, K.; Sang-Kwon, L. Thermal Conductivity Measurements of Single-Crystalline Bismuth Nanowires by the Four-Point-Probe 3-ω Technique at Low Temperatures. *Nanotechnology* **2013**, *24*, 185401.
(22) Lee, W. S.; Won, S.; Park, J.; Lee, J.; Park, I. Thermo-Compressive Transfer Printing for Facile Alignment and Robust Device Integration of Nanowires. *Nanoscale* **2012**, *4*, 3444−3449.
(23) Yi-Kuei, C.; Franklin Chau-Nan, H. The Fabrication of ZnO Nanowire Field-Effect Transistors Combining Dielectrophoresis and Hot-Pressing. *Nanotechnology* **2009**, *20*, 235202.
(24) Qiliang, L.; Sang-Mo, K.; Richter, C. A.; Edelstein, M. D.; Bonevich, J. E.; Kopanski, J. J.; Suehle, J. S.; Vogel, E. M. Precise Alignment of Single Nanowires and Fabrication of Nanoelectromechanical Switch and Other Test Structures. *IEEE Trans. Nanotechnol.* **2007**, *6*, 256−262.
(25) Fan, Z.; Ho, J. C.; Jacobson, Z. A.; Yerushalmi, R.; Alley, R. L.; Razavi, H.; Javey, A. Wafer-Scale Assembly of Highly Ordered Semiconductor Nanowire Arrays by Contact Printing. *Nano Lett.* **2007**, *8*, 20−25.
(26) He, J.-H.; Chang, P. H.; Chen, C.-Y.; Tsai, K.-T. Focused-Ion-Beam-Deposited Pt Contacts on ZnO Nanowires. *ECS Trans.* **2009**, *16*, 13−20.
(27) Lee, W. S.; Choi, J.-h.; Park, I.; Lee, J. Room-Temperature Compressive Transfer Printing of Nanowires for Nanoelectronic Devices. *Langmuir* **2012**, *28*, 17851−17858.
(28) Wei, C.; Beidaghi, M.; Penmatsa, V.; Bechtold, K.; Kumari, L.; Li, W. Z.; Chunlei, W. Integration of Carbon Nanotubes to C-MEMS for On-Chip Supercapacitors. *IEEE Trans. Nanotechnol.* **2010**, *9*, 734−740.
(29) Penmatsa, V.; Kim, T.; Beidaghi, M.; Kawarada, H.; Gu, L.; Wang, Z.; Wang, C. Three-Dimensional Graphene Nanosheet Encrusted Carbon Micropillar Arrays for Electrochemical Sensing. *Nanoscale* **2012**, *4*, 3673−3678.
(30) Maitra, T.; Sharma, S.; Srivastava, A.; Cho, Y.-K.; Madou, M.; Sharma, A. Improved Graphitization and Electrical Conductivity of Suspended Carbon Nanofibers Derived from Carbon Nanotube/Polyacrylonitrile Composites by Directed Electrospinning. *Carbon* **2012**, *50*, 1753−1761.
(31) Sharma, C. S.; Katepalli, H.; Sharma, A.; Madou, M. Fabrication and Electrical Conductivity of Suspended Carbon Nanofiber Arrays. *Carbon* **2011**, *49*, 1727−1732.
(32) Teo, W. E.; Ramakrishna, S. A Review on Electrospinning Design and Nanofibre Assemblies. *Nanotechnology* **2006**, *17*, R89−R106.
(33) Kiselev, P.; Rosell-Llompart, J. Highly Aligned Electrospun Nanofibers by Elimination of the Whipping Motion. *J. Appl. Polym. Sci.* **2012**, *125*, 2433−2441.
(34) Sharma, S.; Sharma, A.; Cho, Y.-K.; Madou, M. Increased Graphitization in Electrospun Single Suspended Carbon Nanowires Integrated with Carbon-MEMS and Carbon-NEMS Platforms. *ACS Appl. Mater. Interfaces* **2012**, *4*, 34−39.
(35) Akl, A. A.; Kamal, H.; Abdel-Hady, K. Fabrication and Characterization of Sputtered Titanium Dioxide Films. *Appl. Surf. Sci.* **2006**, *252*, 8651−8656.
(36) Buha, J. Solar Absorption and Microstructure of C-Doped and H-Co-Doped TiO2 Thin Films. *J. Phys. D: Appl. Phys.* **2012**, *45*, 385305.
(37) Blanco Carballo, V. M.; Melai, J.; Salm, C.; Schmitz, J. Moisture Resistance of SU-8 and KMPR as Structural Material. *Microelectron. Eng.* **2009**, *86*, 765−768.

(38) Cristian, F.; Francisco, H.-R.; Joan Daniel, P.; Román, J.-D.; Teresa, A.; Joan Ramon, M. On the Photoconduction Properties of Low Resistivity TiO2 Nanotubes. *Nanotechnology* **2010**, *21*, 445703.
(39) Wu, N. Effect of Calcination Atmosphere on TiO2 Photocatalysis in Hydrogen Production from Methanol/Water Solution. *J. Photochem. Photobiol., A* **2004**, *163*, 277−280.
(40) Zhu, Z.; Zhang, L.; Howe, J. Y.; Liao, Y.; Speidel, J. T.; Smith, S.; Fong, H. Aligned Electrospun ZnO Nanofibers for Simple and Sensitive Ultraviolet Nanosensors. *Chem. Commun.* **2009**, 2568−2570.
(41) Chen, Y.; Wang, X.; Erramilli, S.; Mohanty, P.; Kalinowski, A. Silicon-Based Nanoelectronic Field-Effect pH Sensor with Local Gate Control. *Appl. Phys. Lett.* **2006**, *89*, 223512.
(42) Zhao, R.; Xu, M.; Wang, J.; Chen, G. A pH Sensor Based on the TiO2 Nanotube Array Modified Ti Electrode. *Electrochim. Acta* **2010**, *55*, 5647−5651.
(43) Li, D.; Wang, Y.; Xia, Y. Electrospinning of Polymeric and Ceramic Nanofibers as Uniaxially Aligned Arrays. *Nano Lett.* **2003**, *3*, 1167−1171.
(44) Li, D.; Wang, Y.; Xia, Y. Electrospinning Nanofibers as Uniaxially Aligned Arrays and Layer-by-Layer Stacked Films. *Adv. Mater.* **2004**, *16*, 361−366.
(45) Deitzel, J. M.; Kleinmeyer, J. D.; Hirvonen, J. K.; Beck Tan, N. C. Controlled Deposition of Electrospun Poly(Ethylene Oxide) Fibers. *Polymer* **2001**, *42*, 8163−8170.